Discussion of assumptions behind the external dynamic models in ship collisions and groundings

Zhaolong Yu [a, b*], Zhenhui Liu [c], Jørgen Amdahl [a, b]

a. Department of Marine Technology, Norwegian University of Science and Technology (NTNU)

b. Centre for Autonomous Marine Operations and Systems (AMOS), NTNU

c. Aker Solutions AS, Trondheim, Norway

Abstract

In the past decades, a prevailing way for the assessment of responses in ship collisions and groundings has been to decouple the problem into two parts: external dynamics and internal mechanics. The external dynamics deals with global motions of the two interacting bodies prior to, during and after the collision. The main outcome of an external dynamics assessment is the energy loss during the collision, which will be dissipated by structural deformations in the assessment of internal mechanics. The decoupled method works well for right-angle collisions in general, but the accuracy can be much less in many scenarios, e.g. skew collisions with small collision angles and collisions with long durations. This is mainly because the assumptions in the decoupled method are violated in the studied cases.

This paper reviews the assumptions and simplifications behind the external dynamic models and discusses validity of the assumptions by comparing with coupled simulation results. Decoupled and coupled models in both planar 3DOF and full 6DOF are addressed. Various collision scenarios are studied, including colliding with oblique plates, grounding on a sloping sea floor, crushing into rigid plates with normal vectors misaligned with coordinate axes, and collision with a submersible platform. In some scenarios, cases with different attack angles and impact velocities are simulated. The outcome will help understand potential limitations of the decoupled method, which should be used with care.

Keywords: collision and grounding; external dynamics models; validity check; impact mechanics; coupled simulation; secondary impacts

1. Introduction

Ship collisions and groundings are highly nonlinear and transient, coupled dynamic processes involving large structural deformations and ship motions. It is still challenging to capture the coupling between structures and the surrounding fluid and to assess accurately the structural responses in accidental collisions and groundings.

In assessing the responses in ship collisions and groundings, a prevailing way is to decouple the problem into two parts: the external dynamics and the internal mechanics, as suggested by Minorsky (1958); refer Fig 1. The external dynamics models simplify the effect of fluid as constant added masses such that the whole collision system is undamped and the principle of conservation of momentum and energy applies. This allows for a fast estimation of the dissipated energy in collisions with reasonable accuracy. A few external dynamic models are available in

* Corresponding author, Dr. Zhaolong Yu
Email: zhaolong.yu@ntnu.no

the literature. Pedersen and Zhang (1998) proposed a closed form analytical model for the planar external dynamics problem. Stronge (2004) developed a solution for three dimensional (3D) impacts between rigid bodies. Liu and Amdahl (2010) applied Stronge's 3D model to investigate ship collision problems, allowing objects with 3D eccentricities and geometries such as icebergs to be considered. The problem of external dynamics in ship collisions has also been addressed in Brown (2002), Popov et al. (1969), Tabri (2012), Zhang et al. (2017), etc.

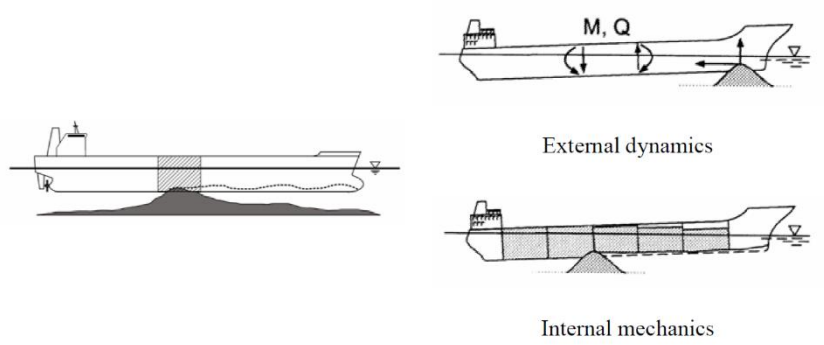

Fig. 1. External dynamics and internal mechanics in ship grounding (Hong, 2009)

The energy loss produced from external mechanics is normally based on the fully plastic impact assumption, where the restitution factor being the ratio of normal velocities before and after impact is set zero. This energy loss is believed to be conservative (Pedersen and Zhang, 1998, Liu and Amdahl, 2010). The lost energy will be dissipated by structural deformations in the assessment of internal mechanics with experiments, numerical simulations and analytical methods e.g. (Oshiro et al., 2017, Wang et al., 2008, Travanca and Hao, 2014), where the struck ship is normally fixed in space, and the striking ship moves along a prescribed path. The final penetration is obtained when the area under the force-penetration curve equals the energy loss resulting from the external dynamic calculations. The procedure described here is termed as the "decoupled method" in this paper. It has been widely used due to its simplicity.

As the decoupled method is based on a few simplifications and neglects the coupling effect between structural damage and ship motions, the method may fail to predict the correct response in certain scenarios, e.g. skew collisions with small collision angles and collisions with long durations. Therefore, a few researchers turn to coupled methods, which yield better representation of hydrodynamic loads and account for ship motions. Examples of the coupled collision simulation models are Brown (2002), Petersen (1982), Tabri et al. (2010), Samuelides and Frieze (1989), Le Sourne et al. (2012) and Pill and Tabri (2011). Until now, the coupled models have not been applied as much as the decoupled method even though the coupled models are more accurate. This is because most coupled models are based on simplifications of collision forces and structural damage, which are of major concern in ship collision assessment. Coupled ship collision simulations using non-linear finite element codes without simplification of the collision force and structural damage can be fulfilled by using either the MCOL routine in LS-DYNA or the user defined load in LS-DYNA. MCOL is a 3D external dynamics program for ship collision embedded in LS-DYNA implemented by French Shipbuilding Research Institute (IRCN) (Ferry,

2001), and some applications of MCOL can be found in (Le Sourne et al., 2001, Le Sourne et al., 2012). Alternatively, Yu et al. (2016a), Yu and Amdahl (2016) and Yu et al. (2016b) adopted the user defined load subroutine in LS-DYNA to implement a traditional maneuvering model and the linear potential flow theory, respectively, into LS-DYNA, fulfilling a coupled ship collision simulation. Letting the linear potential flow theory represent the effect of fluid in LS-DYNA, the transient effects of fluid, global ship motions, collision forces and structural damage can all be predicted with high accuracy.

Coupled simulation methods and experimental methods have been used to discuss the accuracy of the decoupled method. Brown (2002) compared results from a coupled model based on the simplified collision code (SIMCOL) with the planar 3DOF decoupled method by Pedersen and Zhang (1998). Tabri (2012) used results from a coupled approach and experiments by Tabri et al. (2009) to discuss accuracy of the decoupled method. Zhang et al. (2017) used 60 experimental cases to verify energy absorption predicted by the 3DOF decoupled method. They found that the total deformation energy can be predicted reasonably well, but associating this energy with deformations at certain directions cannot be done at the same precision. In some scenarios, the predicted results can be erroneous with respect to damage length and depth.

Previous evaluations of the decoupled method have mainly focused on testing the accuracy of the predicted outcomes, i.e. energy absorption, structural damage, and ship paths, and considerable discrepancies were found in some cases. The discrepancies mainly resulted from violation of the assumptions and simplifications adopted in the external dynamic models, but the assumptions and their validity were seldom discussed in detail in the literature. In addition, the 3DOF decoupled method was of major interest in literature, and little discussion was made on the 6DOF decoupled method.

This paper reviews assumptions and simplifications adopted in the external dynamic models and discusses the validity of the assumptions by comparing the results with those obtained from the 3DOF and 6DOF coupled methods by Yu et al. (2016a), Yu and Amdahl (2016) and Yu et al. (2016b). Various collision scenarios are studied, including collision with oblique plates, grounding on a sloping sea floor, crushing into rigid plates with normal vectors misaligned with coordinate axes, and collision with a submersible platform. In some scenarios, cases with different attack angles and impact velocities are simulated. The outcome will help understand potential limitations of the decoupled method.

2. 6DOF coupled simulation of ship collision and grounding

2.1 Coupled model 1: hydrodynamic forces from maneuvering coefficients

The coupled model 1 uses a traditional ship maneuvering model to represent hydrodynamic forces for the in-plane surge, sway and yaw motions during collisions. The maneuvering model was proposed by Norrbin (1971) with a series of nondimensional coefficients based on Froude scaling. The nondimensional coefficients were determined by Van Berlekom and Goddard (1972) based on experiments. The coefficients can be adjusted according to ship deadweight, length/beam (L/B) ratio and rudder size, such that the model can be applied to a wide range of vessels.

It was assumed that the out-of-plane heave, roll and pitch motions, were not coupled with the in-plane ship motions and there was no coupling among roll, pitch and heave motions. The latter were simplified as three single-degree-of-freedom spring damper vibration subsystems. More details of the coupled model 1 can be found in Yu et al. (2016a) and Yu and Amdahl (2016).

2.2 Coupled model 2: hydrodynamic forces from the linear potential flow theory

The coupled model 2 uses linear potential flow theory with and without considering the forward speed effect to calculate hydrodynamic loads during collisions.

The forces acting on a ship during collision and grounding accidents are the results of the propeller and rudder forces, hydrodynamic forces and collision forces. Before collision, propeller and rudder forces are in equilibrium with the hydrodynamic forces acting on the hull. Departure from this state due to a sudden change in the external forces causes a change in the hydrodynamic forces acting on the hull (Petersen, 1982). The governing equilibrium equations are:

$$\sum_{k=1}^{6}\left[\left(M_{jk}+A_{jk}(\infty)\right)\ddot{\eta}_k+\int_0^t K_{jk}(t-\tau)\cdot\left[\dot{\eta}_k(\tau)-\dot{\eta}_k(t=0)\right]d\tau+C_{jk}\eta_k\right]=F_j(t)\left(j=1,2,...,6\right) \quad (1)$$

where M_{jk}, $A_{jk}(\infty)$, and C_{jk} are components of the generalized ship mass matrix, the added mass of infinite frequency and the restoring matrix of the ship. The index $j=1,...,6$ represents surge, sway, heave, roll, pitch and yaw, respectively. $\dot{\eta}_k(t=0)$ is the velocity component of the striking ship in the k_{th} degree of freedom just before impact and $F_j(t)$ is the generalized collision force in the j_{th} degree of freedom. $\int_0^t K(t-\tau)\cdot\dot{\eta}(\tau)d\tau$ is the convolution integral connected with free-surface memory effects and $K_{jk}(t)$ is the so called impulse-response or retardation function connected with direction *j* and *k*.

The forward speed effect can influence ship hydrodynamic forces in several aspects. First, a forward speed will modify the time derivative bringing in a convective term to the Bernoulli equation. This gives an explicit change in the pressure. An implicit variation is caused by the changes in the boundary value problem for the velocity potential. In particular, the free surface and body boundary conditions change when the forward speed effect is accounted for. The forward speed will also modify the frequency felt by the ship when interacting with incident waves. This encounter frequency effect is not included as normally no incident waves are assumed in ship collision and grounding problems. The governing equations of ship motions considering the forward speed effect are given by:

$$\sum_{k=1}^{6}\begin{bmatrix}\left(M_{jk}+A_{jk}(u,\infty)\right)\ddot{\eta}_k+B_{jk}(u,\infty)\left[\dot{\eta}_k(\tau)-\dot{\eta}_k(t=0)\right]\\ +C_{jk}\eta_k+\int_0^t K_{jk}(t-\tau,u)\cdot\left[\dot{\eta}_k(\tau)-\dot{\eta}_k(t=0)\right]d\tau\end{bmatrix}=F_j(t)\left(j=1,2,...,6\right) \quad (2)$$

where the impulse response functions are estimated in terms of the damping coefficients as:

$$K_{jk}(t,u)=\frac{2}{\pi}\int_0^{\infty}\left[B_{jk}(u,\omega_e)-B_{jk}(u,\infty)\right]\cos(\omega_e t)\,d\omega_e \tag{3}$$

The impulse-response function can be expressed as a combination of speed-independent and speed-dependent contributions. The retardation function can thus be expressed as:

$$K_{jk}(t,u)=K_{jk}^{0}(t)+uK_{jk}^{u}(t)+u^2K_{jk}^{u^2}(t)+\delta K_{jk} \tag{4}$$

More details with respect to the coupled model 2 can be found in Yu et al. (2016b).

2.3 Implementation and verification

The hydrodynamic models were implemented into LS-DYNA by the use of the user defined load subroutine (LOADUD) and user common variable (USERCOMM). The hydrodynamic forces are calculated every 0.001s, and this is much larger than the structural time step in the order of 10^{-6}s. In this way, hydrodynamic forces, structural deformations and ship motions were coupled efficiently.

Implementation of the coupled models was verified by comparing with SIMO simulation and a user code considering the forward speed effect. SIMO (Marintek, 2012) is a computer program for the simulation of motions and behaviors of floating vessels, which gives a transient solution. Added masses and damping coefficients calculated with the potential flow theory can be directly imported into SIMO. The collision forces were extracted from the coupled simulation, and applied as external forces on the ship in SIMO and the user code. The obtained ship motions were compared with those from the coupled simulation. Because SIMO cannot consider the forward speed effect, we developed a user code to solve the motion equations considering the forward speed effect, and verified the code against SIMO for cases without considering the forward speed. Results showed that ship motions of the coupled models agreed well with those by SIMO and the user code. Excellent agreement was found especially for coupled model 2 with linear potential flow theory. The accuracy of coupled model 1 is less, but is acceptable for ship collision simulation. Fig. 2 shows snapshots of ship motions in collision scenario 4 (see *section 3.3*) using the coupled model 2. All the 6DOF ship motions can be clearly observed and complicated ship trajectories are well captured, demonstrating the soundness of the implementation. The details can be referred to Yu et al. (2016a), Yu and Amdahl (2016) and Yu et al. (2016b).

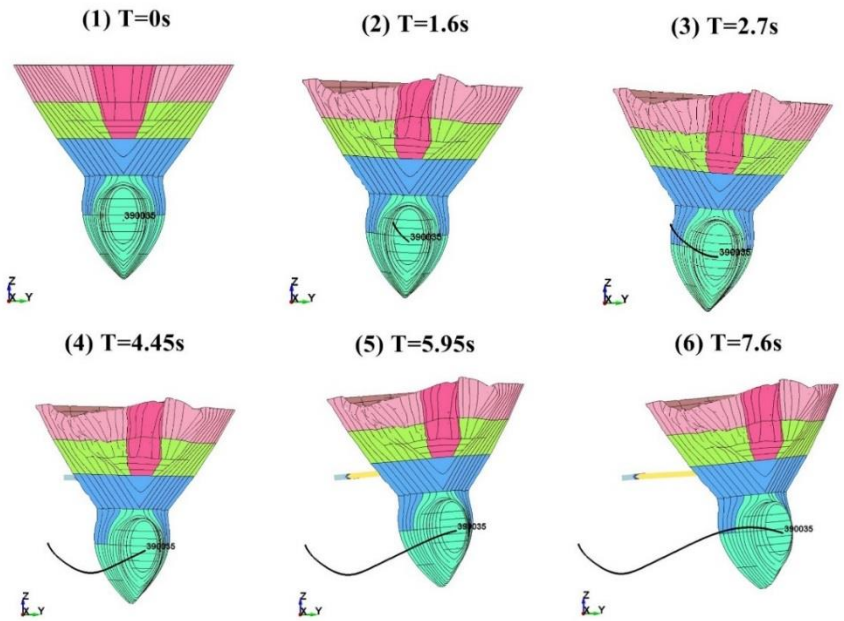

Fig. 2. Snapshots of a coupled collision simulation using model 2 (Yu et al., 2016b)

3. Model description and case studies

With the proposed coupling models, an offshore supply vessel colliding with several rigid walls with different orientations and a semisubmersible platform is simulated. The rigid wall is modelled with much larger extension than the vessel. The ship and semisubmersible models and the collision scenarios are described.

3.1 The striking ship

The striking ship is a 7500-ton modern supply vessel with a bulbous bow. The bow FE model is shown in Fig. 3. The element size is generally 120 mm. The plate thickness varies from 7 mm for the decks to 12.5 mm in the bulb. The stiffener spacing is approximately 600 mm, with ring stiffeners and breast hooks of approximately 250 × 15 mm in the bulb. The bulbous part is almost cylindrical and is relatively strong. The forecastle protrudes 1.2 m ahead of the bulb.

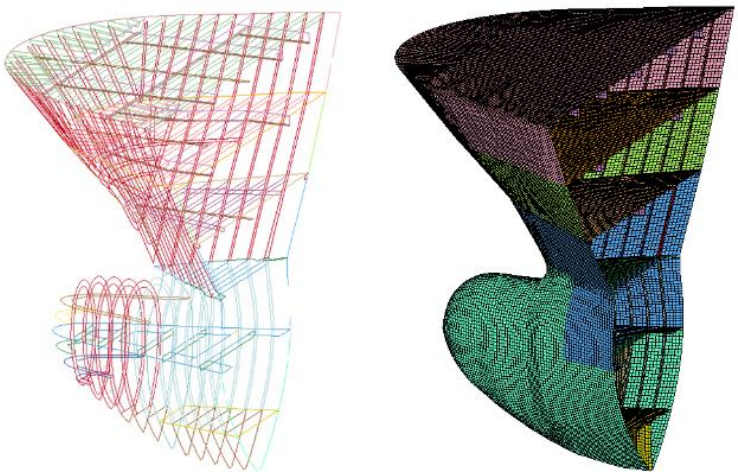

Fig. 3. The FE model of the bulbous bow

The ship's hull girder is represented by a long rigid beam from the bow back towards the centre of gravity of the vessel; see Fig. 4. The rigid beam and the deformable ship bow are connected to a rigid shell plate at the rear of the bow model. The beam properties are calibrated to represent correctly the total mass and inertia of the ship with respect to the centre of gravity taking into account the contribution of the bow model. The 6DOF hydrodynamic forces and moments are applied as user-defined loads at the COG of the ship. Because the user defined load subroutine does not allow applying bending moments directly, the bending moments have to be transformed into force pairs. Therefore, several small rigid beams are created for applying bending moments in roll, pitch and yaw. The interaction of the beams is located at the centre of gravity (see Fig. 4).

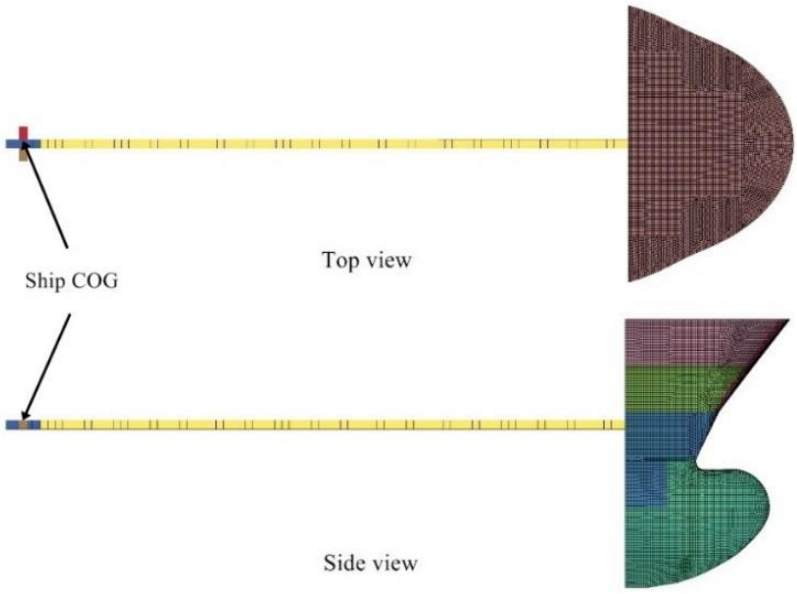

Fig. 4. The FE model of the striking ship

3.2 The semisubmersible platform

The platform is a four-legged semisubmersible with ring-pontoons. Only the front part of the column including the sponson is modelled; see Fig. 5. The model has mesh size in the range of 90 mm in the region where large deformations are expected. This gives on average three elements over a stiffener web and minimum five elements in the plate between each stiffener. Gross plate thickness including corrosion allowance is used, with thickness in the platform shell between 18 and 25 mm. Vertical stiffeners are spaced 640 mm apart, and are of types HP280 and HP300 in the impacted region. Inside of the sponson, HP260 stiffeners are applied. The stiffeners are modelled as flat bars, disregarding the actual bulb. Thus, the shear capacity of the stiffener is maintained, but the bending stiffness from the bulb is disregarded in the model discretization.

The mass of the platform is considerably larger than that of the striking ship. Hence, the platform motions are very small and are therefore neglected for simplicity. Global motions are assumed to have little interaction with local deformations. The nodes on platform boundary edges marked in black in Fig. 5, are constrained against all translations and rotations. The ship and platform steel materials with power law hardening are used, and the parameters are shown in Table 1. Two schemes of contacts are used in FE simulations, namely self-contact and master-slave contact. Two pairs of self-contact are defined, one for the vessel and one for the platform. This enables contact between parts of the bodies if they should deform onto itself. A master-slave contact definition is applied between the vessel and the platform, and acts as the main contact. The automatic single surface and automatic surface to surface contacts in LS-DYNA is used. Static contact friction is set to 0.3 for all contacts.

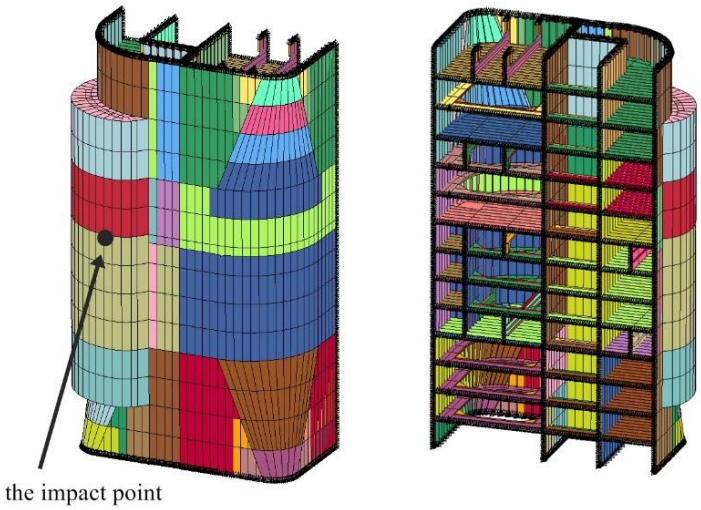

Fig. 5. FE models of the semi-sub platform column

Table 1. The steel material used in the ship and platform

	Young modulus E (MPa)	Poisson ratio ν	Yield stress σ_y (MPa)	Power law K (MPa)	Power law n

Ship	2.07×10^5	0.3	275	830	0.24
Platform	2.07×10^5	0.3	420	760	0.16

3.3 Definition of collision scenarios

The studied situation is that a 7500-ton supply vessel runs into rigid plates with different orientations and a semisubmersible platform. Five scenarios are defined as shown in Fig. 6. The scenarios are (1) colliding with oblique plates, (2) grounding on a sloping sea floor (3) crushing into rigid plates with the normal vector of $\vec{n}_1 = [-0.74, 0.24, 0.63]$, (4) crushing into rigid plates with the normal vector of $\vec{n}_2 = [-0.86, 0.42, -0.30]$, (5) collision with a submersible platform. In the scenarios, several cases may be simulated with different attack angles and impact velocities.

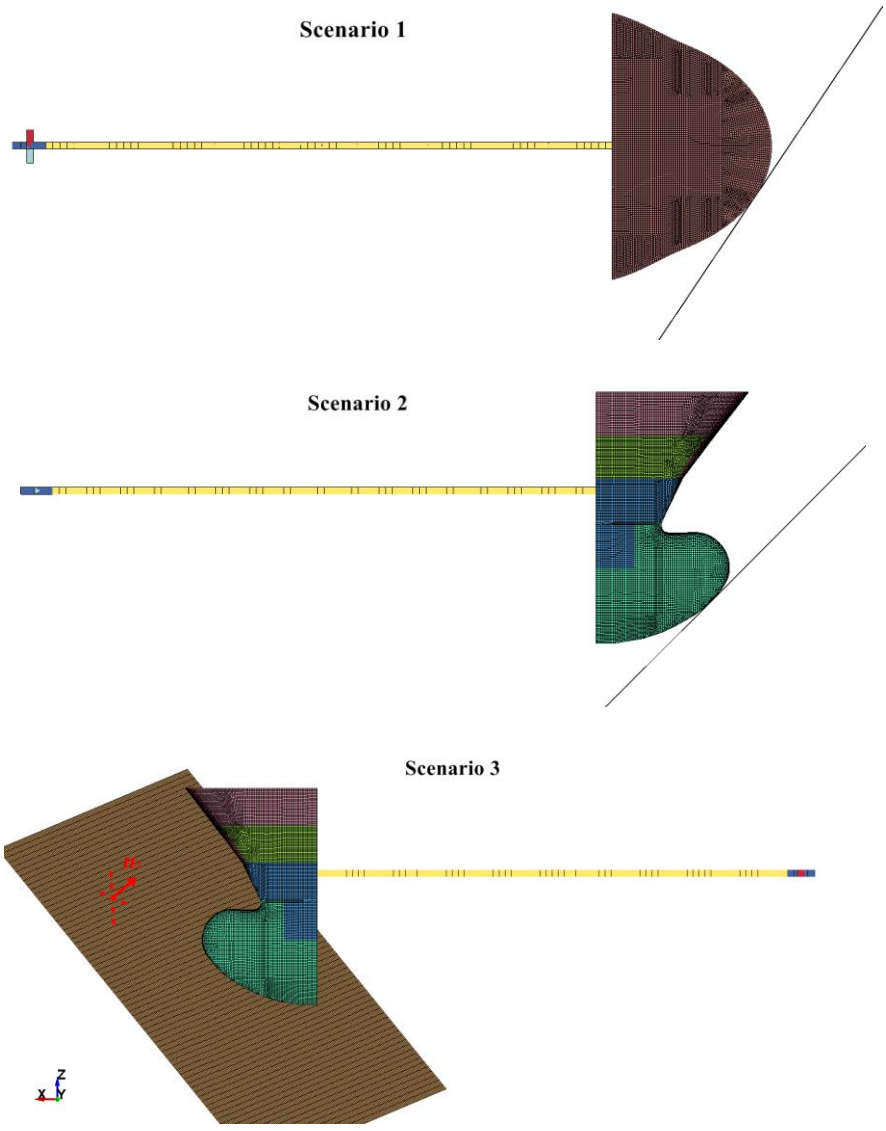

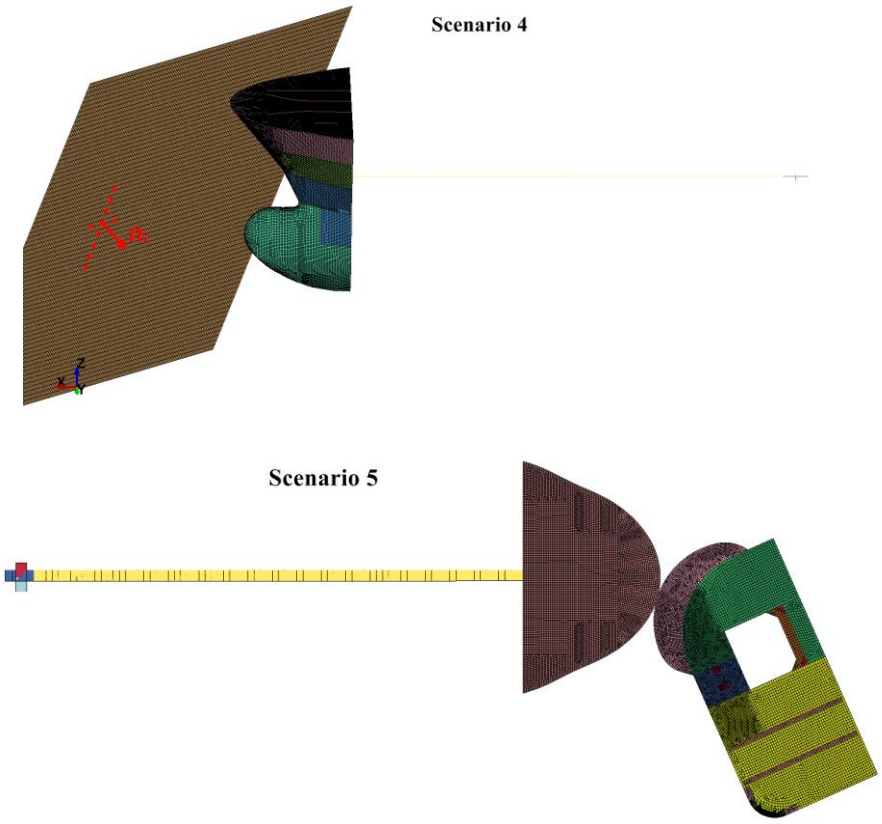

Fig. 6. The collision scenarios

4. Discussion of assumptions behind the external dynamic models

When evaluating validity of the assumptions behind the external dynamic models, simulation results from the coupled models are assumed as the 'true' results. Discussions are made by comparing results with those from coupled simulations.

4.1 Basic assumptions of the external dynamic models

Pedersen and Zhang (1998) proposed an external dynamic model considering the planar 3DOF motions, i.e. surge, sway and yaw; refer Fig. 7(a). A local coordinate ξη system is established with the ξ direction normal to the contact point. The ships are allowed to rebound from each other in the ξ direction by introducing a coefficient of restitution e. The relative velocity in the ξ direction at the end of the impact can be directly obtained as $-e\cdot\dot{\xi}(\mathrm{t}=0)$. The parameter e is 0 for an entirely plastic collision and is 1 for a perfect elastic collision. The ratio of impact impulses in the η and ξ directions $\mu = I_{\eta 0} / I_{\xi 0}$ is introduced to judge whether the striking and struck ships will stick or slide against each other. The definitions of $I_{\eta 0}$ and $I_{\xi 0}$ can be referred to Pedersen and Zhang (1998).

If $|\mu| \le |\mu_0|$ (μ_0 is the friction coefficient), the two ships will stick together, and the relative velocity after collision is zero in the η direction. The collision forces are assumed to satisfy the relation $F_\eta = \mu \cdot F_\xi$, where μ is the ratio of impact impulses.

If $|\mu| > |\mu_0|$, the two ships will glance off each other. Then, $F_\eta = \mu_0 \cdot F_\xi$ according to Coulomb's friction law.

With these assumptions, the relative velocities in the ξ and η directions and the subsequent dissipated energy after the collision are readily obtained. Liu and Amdahl (2010) extended the external dynamic model to consider the full 6DOF motions based on Stronge (2004)'s 3D model. The collision forces are given in the right-handed global XYZ coordinate as defined in Fig. 7(b). It is assumed that the normal and tangential friction factors μ_n and μ_t are constant and are given as

$$\mu_n = sign(dp_1)\frac{\sqrt{dp_1^2 + dp_2^2}}{dp_3} \tag{5}$$

$$\mu_t = \frac{dp_2}{dp_1} \tag{6}$$

where dp_1, dp_2 and dp_3 are the impulses in each direction in the local coordinate in Fig. 7 (b), and the definitions can be found in Liu and Amdahl (2010). For sliding cases, μ_n is assumed to be equal to the friction coefficient μ_0. For both models, it is implicitly assumed that the collision angles do not change during the collision process.

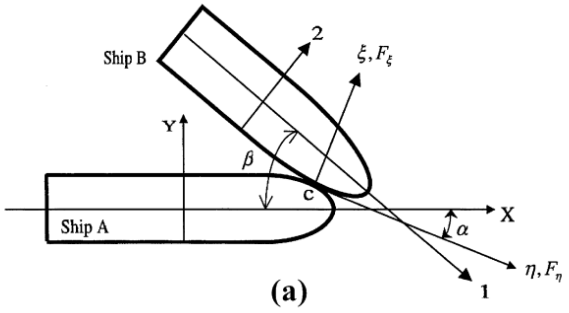

(a)

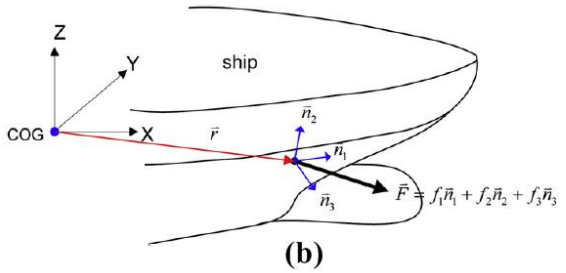

(b)

Fig. 7. External dynamic models (a). 3DOF model by Pedersen and Zhang (1998); (b). 6DOF model by Liu and Amdahl (2010)

4.2 Discussions

4.2.1 The assumption of constant added masses

The external dynamic models are based on conservation of energy and momentum. However, ship collision including the surrounding water is not an undamped system considering the wave making damping, viscous damping, etc.

The problem of solving the hydrodynamic loads acting on ships during collision is often treated as a radiation problem; i.e. no incident waves and currents are considered. From linear potential flow theory point of view, ship collision forces will excite ship motions in different frequencies. For each frequency, there exist certain added mass and damping matrices with coupling terms among different DOFs. Fourier transformation of the collision forces is useful to check the frequency content. The single-sided amplitude spectrums of the collision forces in scenario 3 and scenario 4 with an impact velocity of 2.78 m/s are plotted in Fig. 8. The frequency distribution is quite dispersive, and the amplitudes are considerable from low frequencies to high frequencies with respect to ship motions. It is difficult to find a representative frequency to determine the constant added masses as inputs of the external dynamic models; In addition, as collision occurs when the two bodies are extremely close, fluid multi-body interactions may become significant.

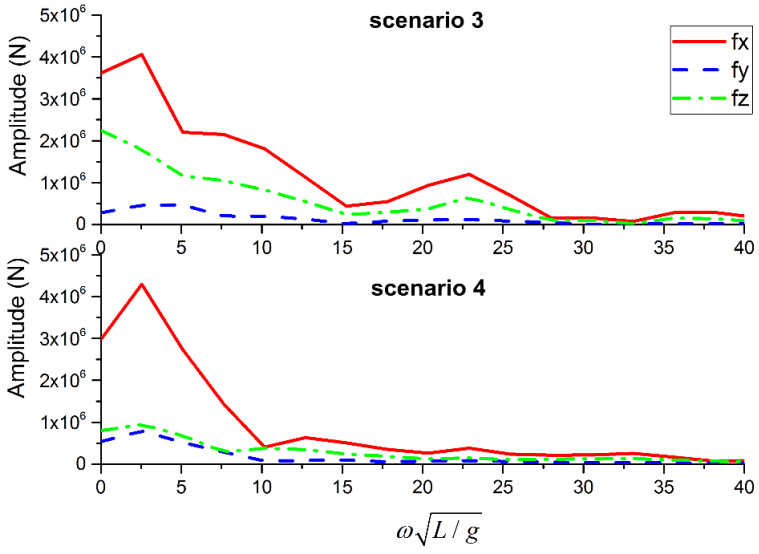

Fig. 8. Single-sided amplitude spectrum of collision forces

The selection of constant added mass coefficients is not straightforward and will introduce errors as well. Minorsky (1958) proposed a constant value of 0.4 for the added mass coefficient in sway. Liu and Amdahl (2010) adopted the empirical equations by Popov et al. (1969), which were derived for the purpose of investigating ice loads exerted on ship structures. The expressions were functions of ship dimensions given by:

$$
\begin{aligned}
m_{asurge} &= 0 \\
m_{asway} &= 2T / B \\
m_{aheave} &= 2/3\left(BC_{wp}^2\right) / \left(TC_b\left(1+C_{wp}\right)\right) \\
m_{aroll} &= 0.25 \\
m_{apitch} &= B / \left(T\left(3-2C_{wp}\right)\left(3-C_{wp}\right)\right) \\
m_{ayaw} &= 0.3+0.05L / B
\end{aligned}
\tag{7}
$$

where T is the ship draught, B is the width, L is the length, C_{wp} is the water plane coefficient, C_b is the block coefficient, and C_m is midship section coefficient.

Petersen and Pedersen (1981) suggested that the added mass coefficient for sway motion could be estimated from:

$$
m_{asway} = m(\infty) + k\left[m(0) - m(\infty)\right] \tag{8}
$$

where $m(\infty)$ and $m(0)$ are the added mass with infinite frequency and zero frequency. The factor k is a function of collision duration and ship draught.

Motora et al. (1971) presented a theoretical solution for the equivalent added mass coefficients in ship collisions and conducted model experiments on an atomic powered ship of Japan to verify the experimental model. Three equivalent added mass concepts were proposed as follows, which give the exact values of acceleration, momentum and absorbed energy at the end of collisions, respectively.

$$
M + m' = \frac{f(\mathrm{t})}{a(t)} \tag{9}
$$

$$
M + m'' = \frac{\int_0^t f(\tau) d\tau}{v(t)} \tag{10}
$$

$$
M + m''' = \frac{\int_0^t f(\tau) v(\tau)\, d\tau}{\frac{1}{2} v^2(t)} \tag{11}
$$

where M is the ship mass, m', m'' and m''' are the equivalent added masses, and $a(t)$ and $v(t)$ are acceleration and velocity of the vessel at the end of the collision, respectively.

They showed that the equivalent added mass changed with the shape of collision resistance curves, collision duration and the definition of equivalent added mass; refer Fig. 9. Normally, the added mass based on energy similarity should be used. If the duration is infinitely small, the

equivalent added mass is equal to added masses of infinite frequency. The equivalent added mass increases as the duration gets larger. Jia and Moan (2010) studied the equivalent added mass using similar approaches, and found that the added mass was also related to the impact position and the flexibility of the hull girder.

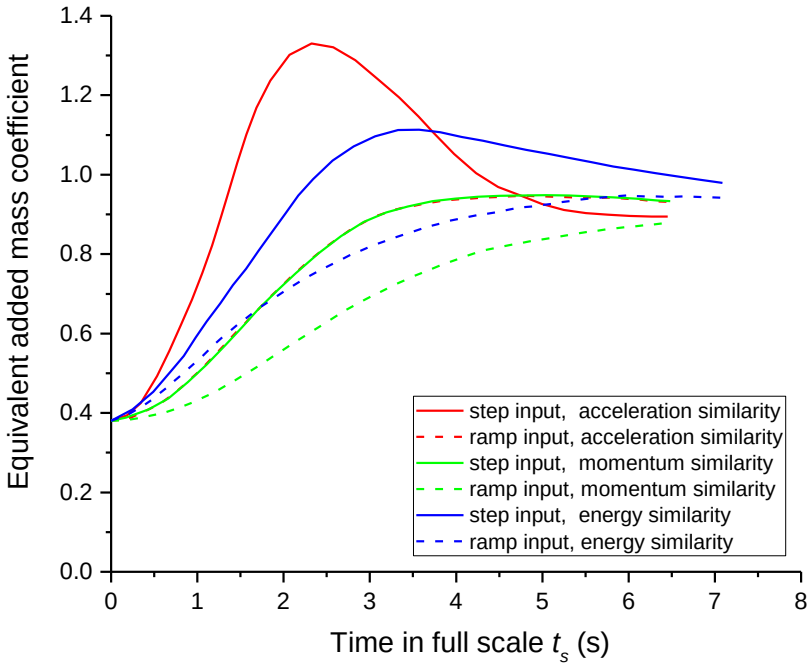

Fig. 9. Equivalent added masses in sway based on the similarity of acceleration, momentum and absorbed energy, under step and ramp input forces (Motora et al., 1971)

The sensitivity of dissipated total energy to added mass coefficients is checked using collision scenario 1 with a collision angle of 35° and 56°. An initial impact velocity of 2.25m/s is assumed, which gives a kinetic energy of about 20 MJ considering the added mass effect. Fig. 10 plots the dissipated total energy predicted by the 6DOF external dynamic model with varying sway and yaw added mass coefficients ranging from 0.3 to 1.0. The maximum and minimum values of dissipated energy are marked with green triangles. The extreme values are reached when added mass coefficients in sway and yaw share the same value of 1.0 and 0.3, respectively.

The dissipated total energy increases with added mass coefficients. The differences between the maximum and minimum values of dissipated energy are about 1.4 MJ and 1.1 MJ, corresponding with an error of 22% and 7% for the two cases. The differences are similar in absolute value, but the relative error increases with decreasing collision angles. The influence of varying added mass coefficients in sway and yaw on the total energy absorption is minor for large collision angle cases, but tends to become important with decreasing collision angles.

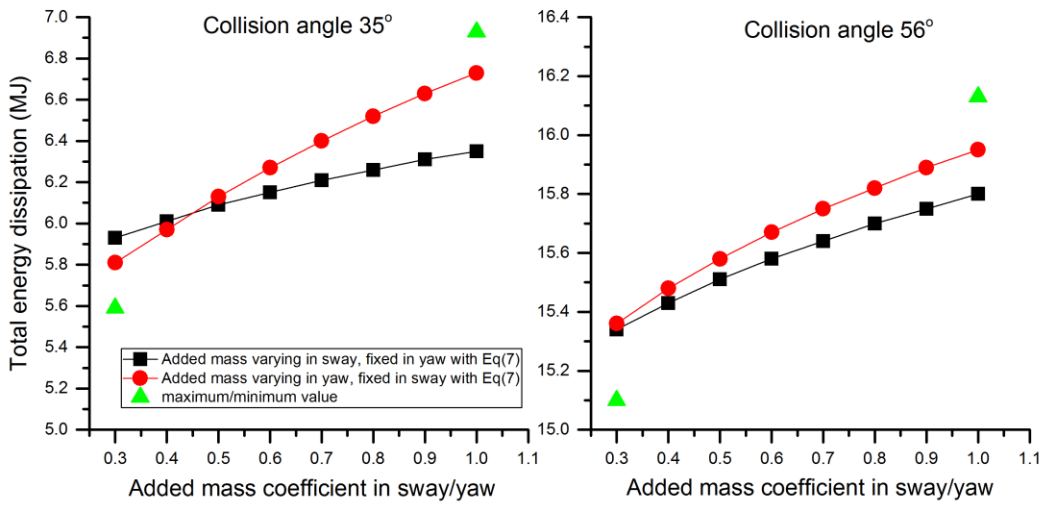

Fig. 10. Variation of dissipated total energy with sway and yaw added mass coefficients

4.2.2 The assumption of proportionality of impulses

In the external dynamic models, the impulses in the normal and tangential directions are assumed to be proportional as described by the normal and tangential friction factors in *Section 4.1*. The validity of this assumption is checked by means of coupled numerical simulations.

Scenario one is studied, where the supply vessel collides with oblique rigid plates with collision angles α=35°, 44°, 56° and 80°, refer Fig. 11. The first three collision angles represent sliding cases while the 80° case is a sticking case. Three coordinate systems are used, i.e. global earth fixed coordinates, ship fixed coordinates and local coordinates at the impact point.

- *3DOF external dynamic model*

In the first place, the 3DOF coupled and decoupled models are used meaning that the roll motion, which can be significant in this scenario, is neglected. Collision forces of the 35° and 56° cases are plotted in the earth-fixed $X_0O_0Y_0$ coordinates in Fig. 12. The collision forces change drastically at about 1.3 s for the collision scenario 56° because the bulbous bow starts to be crushed. During sliding, the Coulomb's friction law gives $F_\eta = \mu_0 \cdot F_\xi$. When transformed into the global coordinate system, the ratio of the vertical and horizontal forces becomes:

$$\lambda = \frac{F_{Y_0}}{F_{X_0}} = \frac{F_\xi \cdot \cos\alpha - F_\eta \cdot \sin\alpha}{F_\xi \cdot \sin\alpha + F_\eta \cdot \cos\alpha} \tag{12}$$

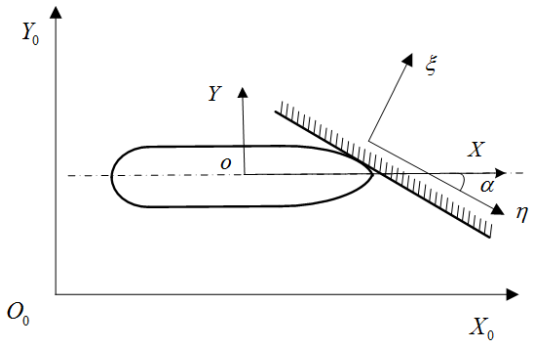

Fig. 11. The coordinate systems

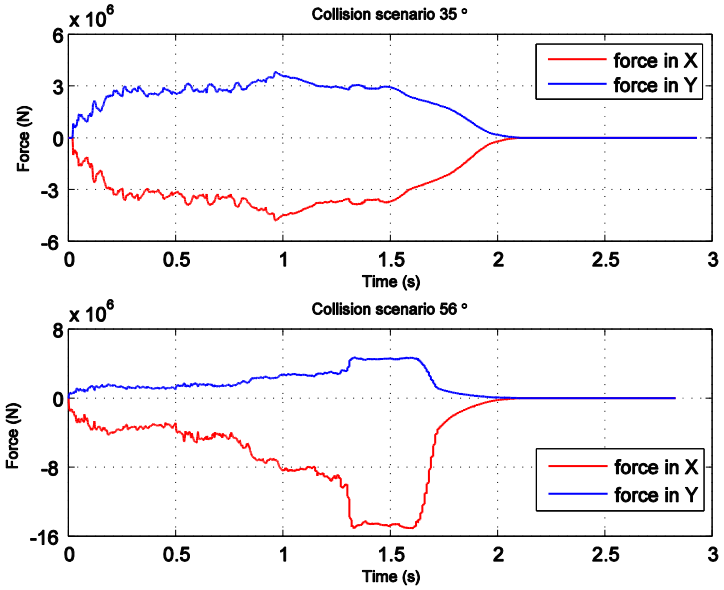

Fig. 12. The time sequence of collision forces in the global coordinate system

$\mu_0 = 0.3$ is used in the simulation, and this gives the curve of force ratio versus collision angle in the global coordinate system in Fig. 13, which can be used to check collision angle changes during collisions. Note that this ratio is only valid for sliding cases. The force ratio curves for collision cases of 35° and 56° are plotted in Fig. 14. Despite some small oscillations, the force ratio generally remains a constant value. According to Fig. 13, the external dynamics model predicts force ratios of 0.31 and 0.79 for collision angles of 56° and 35°, respectively. These values agree well with simulation results shown in Fig. 14. The same also goes for collision case 44°, which confirms the validity of the assumption of a constant force ratio for the sliding cases in the 3DOF external dynamic model.

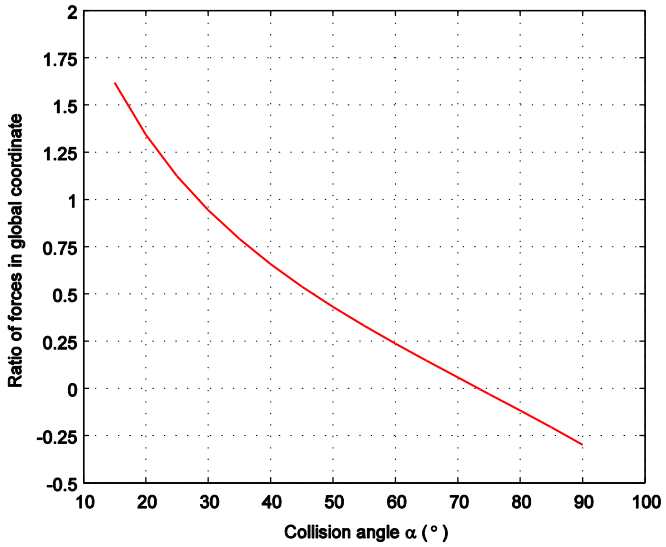

Fig. 13. The ratio of forces versus collision angles in the global coordinate system

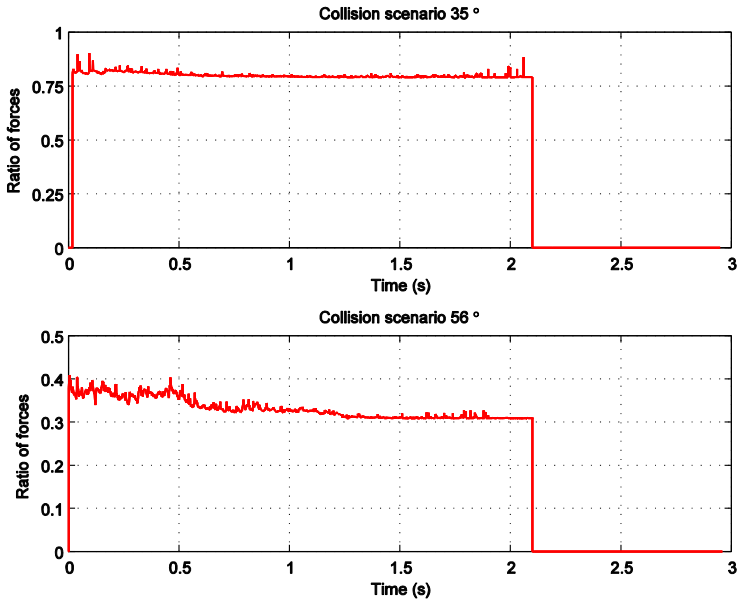

Fig. 14. The ratio of vertical and horizontal forces in the global coordinate system

For the sticking 80° case, the force ratio is approximately $\mu = I_{\eta 0} / I_{\xi 0} = 0.18$ in the local ξη coordinate system and is about 0 when transformed to the global coordinate system with Eq. 12. Collision forces in the longitudinal and transverse directions and the force ratios with the coupled method are plotted in Fig. 15. It is observed that the force ratio varies significantly but remains within ±0.1. The proportionality of impulses is not strictly satisfied in the sticking case, but the mean value of the force ratio may be acceptable.

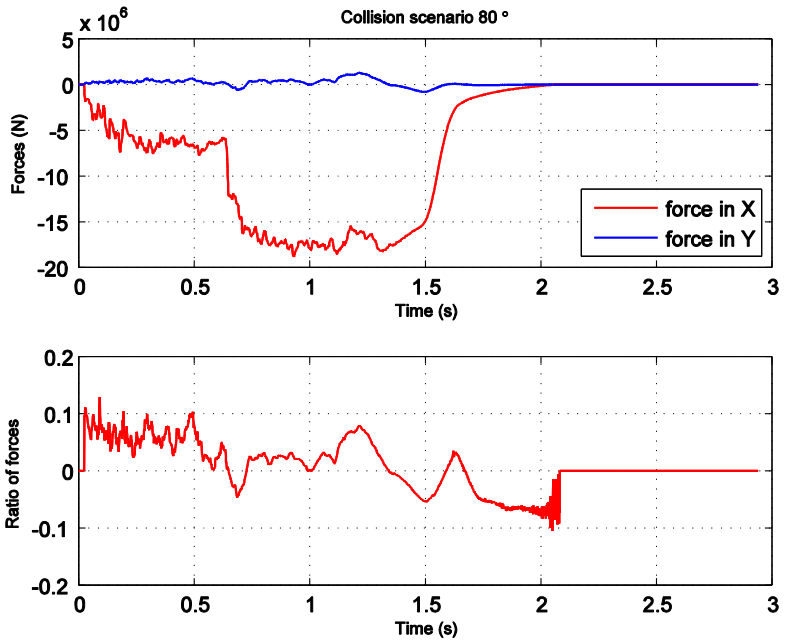

Fig. 15. The collision forces and force ratio for the 80º sticking case

- *6DOF external dynamic model*

In the 6DOF coupled and decoupled methods, the roll motion is taken into account. Fig. 16 plots time histories of the roll and the yaw angles in the 44º and 56º cases for the coupled simulations. The yaw and roll motions are more intense in the 44º case, because in the 56º case, the bulbous bow gets involved in the collision process, which gives a large roll moment that tends to counteract the one produced by deformation of the forecastle, yielding a small resultant bending moment in roll.

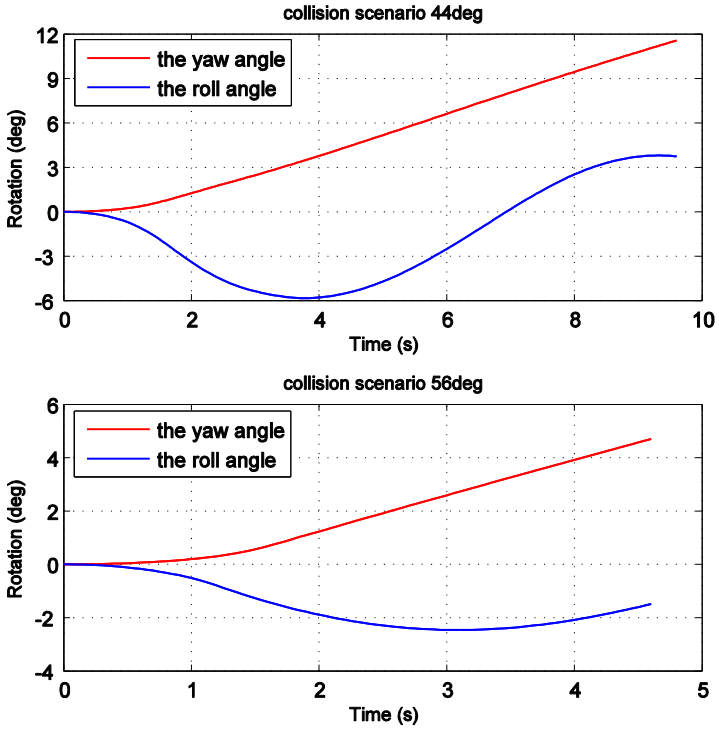

Fig. 16. The time history of roll and yaw angles during collision for the 6DOF coupled method

The collision forces and ratios of impulses for the 44° case with the coupled methods are presented in Fig. 17. The peak forces using the 3DOF and 6DOF coupled methods are quite similar, but the peak values last shorter when the roll motion is considered. This is because the roll motion gives a velocity at the collision point that tends to separate the contact. It is interesting to find that when the 6DOF coupled model is used, the collision force drops to zero at 2.1s and rises up again at 2.8s, and a secondary impact occurs. A detailed explanation of the secondary impact phenomenon is given in *Section 5.1*. The secondary impact significantly extends the entire collision duration, but shortens the first impact duration.

From Fig. 17, the normal friction factor μ_n is almost constant despite small oscillations, and is equal to the sliding friction coefficient 0.3. This is consistent with the findings for the 3DOF models. However, the tangential friction factor μ_t is not quite constant from numerical simulations. This indicates that the ship direction keeps changing on the tangential plane during the impact. The used friction factor μ_t in the external dynamic model can be considered as an averaged (nominal) factor. This may lead to inaccurate energy predictions in the n_1 and n_2 directions, but the sum of energy dissipation in the n_1 and n_2 directions can still be acceptable. In fact, determination of μ_t for the sliding case is not straightforward, and the treatment of the μ_t factor in Liu and Amdahl (2010) does not have solid basis. More investigations should be performed.

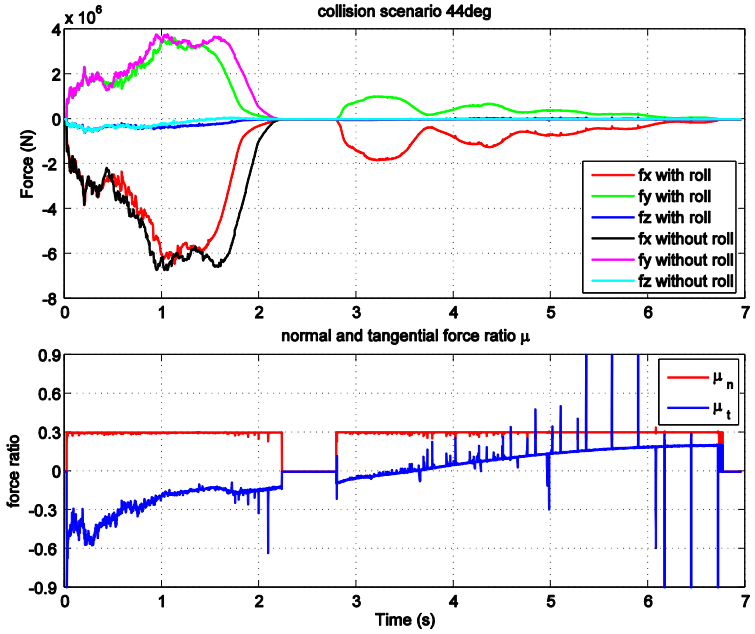

Fig. 17. The collision forces and impulse ratios for the 44° case

4.2.3 The assumption of small collision duration and constant collision angle

Although external dynamic models consider momentum changes in different motions, the initial collision configuration is always used by assuming that collision duration is short and changes of the collision angle during collision are negligible; otherwise numerical iterations will be needed.

Fig. 18 shows ship motions of scenario 1 using the 3DOF coupled model. The collision durations are about 2-3s, which is small compared to the natural periods of the ship motions and may be accepted as short durations. The collision angle changes within this time period are generally within 3° due to the yaw motion. However, if the 6DOF coupled model is used, the roll motion can be considered and a secondary impact occurs. The collision duration is significantly prolonged, and the yaw motion can be as large as 10° at the end of secondary impacts as shown in Fig. 16. This leads to large collision angle changes.

The curved geometries of the striking and struck objects may also change the collision angle during collisions. Fig. 19 shows the sliding collision scenario 5 between a supply vessel and a semisubmersible platform with a collision angle of 56°. The collision resistances and the force ratios are compared in Fig. 20. The duration of the collision process (about 5s) is much longer than that in the 56° rigid plate collision. Unlike the rigid plate collision case, the force ratio μ_n oscillates more intensively. In the first 2 seconds, it oscillates about a mean value of 0.28. This value is close to 0.31 predicted by the decoupled method. However, the force ratio decreases significantly after 2s and oscillates intensively about zero until the end of the collision, which corresponds to a collision angle of 73° according to Fig. 13. The change of the collision angle is considerable and is mainly due to the curved geometry of the struck object and the deformation of both structures.

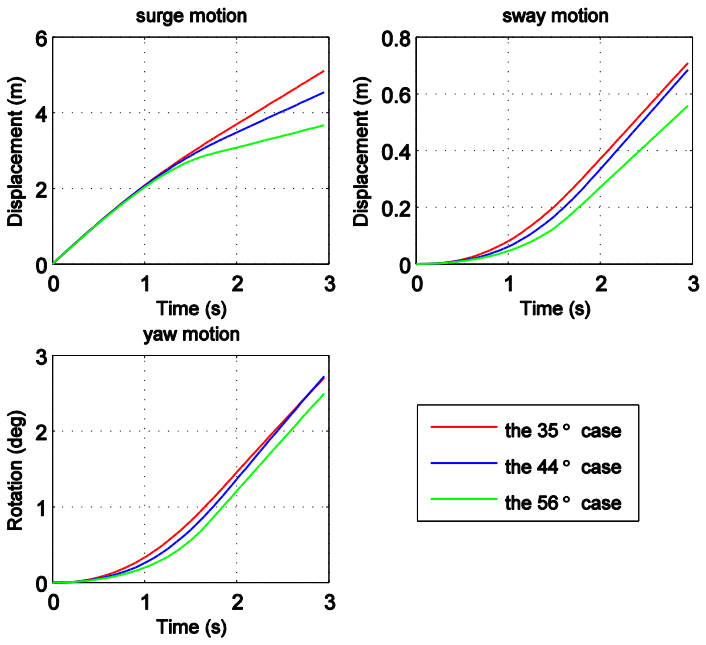

Fig. 18. Ship motions in scenario 1 based on the 3DOF coupled model

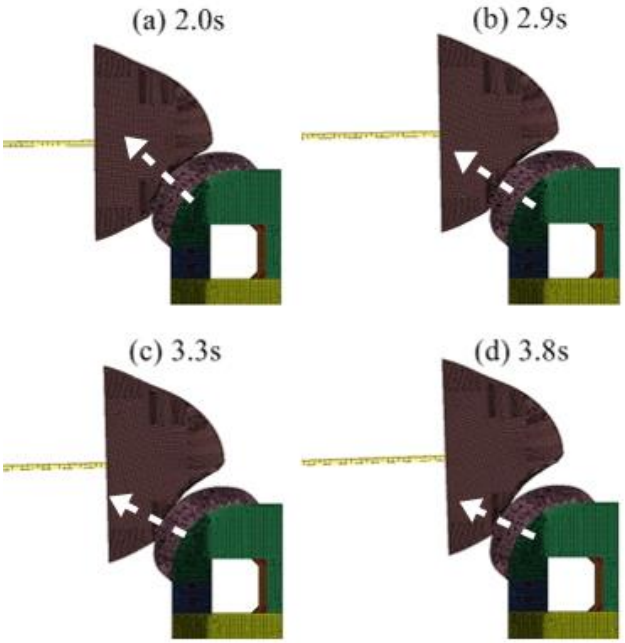

Fig. 19. Snapshots during ship collision with the semisubmersible platform (6DOF model)

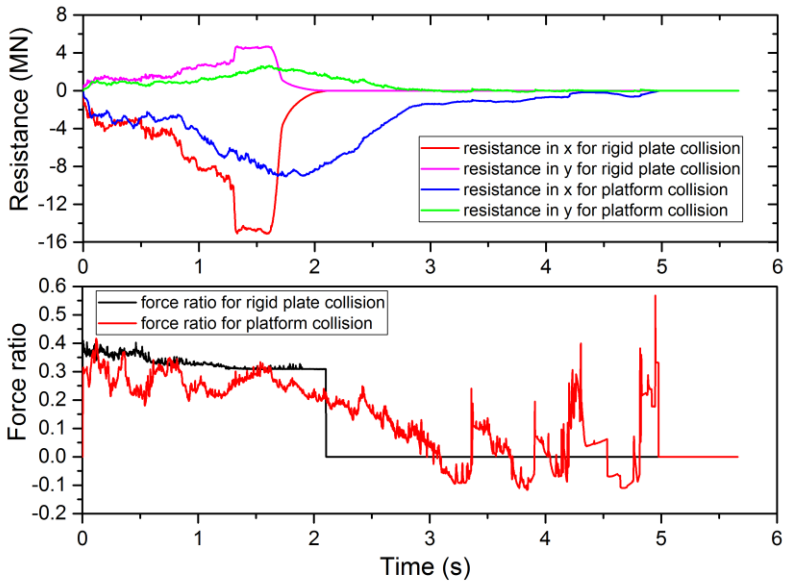

Fig. 20. A comparison of the collision resistances and force ratios μ_n for ship-platform and ship-rigid plate collisions with a collision angle of 56° (6DOF model)

4.2.4 Determination of the normal vector of the contact plane

In the impact mechanics models, it is assumed that collisions occur between rigid bodies, and the striking and struck objects have a common contact plane at the contact point, thus a unique normal vector can be found. However, the colliding bodies are deformable in reality and the initial surfaces of both bodies do not necessarily share a common tangent plane before impact. It is therefore not straightforward to determine the input normal vector for the 3D external dynamic model. The normal vector may be based on either the undamaged surface of the striking or the struck object at the contact point.

It may be considered to use the stronger object to determine the normal vector. For example, for ship collisions with rigid plates in scenarios 1 - 4, the normal vector should be determined by the orientation of the rigid plates. For supply vessel-platform collisions in scenario 5, the normal vector is given by the stronger platform. Good accuracy is obtained in these cases. However, it is not always correct to use the normal vector of the stronger object as input. For example, if a rigid ship bow is assumed in scenario 5, the ship penetrates into the platform shell, and the platform deformation follows the shape of the bow front (see Fig. 21). The out-of-plane ship motions are locked by the deformation of the platform, and little 3D effects are observed. This is somewhat analogous to bow collision with a ship side, where the ship side is weaker and deforms significantly. Fig. 22 compares energy dissipation from the coupled simulation with predictions from the external dynamic model with normal vectors from both the ship bow and the platform. It is found that the normal vector from the weaker platform gives the best results. The internal and friction energy are underestimated to some extent mainly due to effect of the curved geometries leading to an error of 15%-20% for the studied case; refer *Section 4.2.3*. Failure to identify the correct normal vector will yield inaccurate estimation of energy dissipation.

It requires good engineering judgements to determine the appropriate normal vector. From the limited simulation results, it may be recommended to use the normal vector of the initial surface of the stronger structure as the input. This should be valid when 6DOF ship motions are not restricted by structural deformations. In practice, ship motions may potentially be locked by structural deformations to different extents. An example can be seem from the coupled ship-jacket leg collision simulation in Fig. 23 reported in Yu and Amdahl (2018). This motion locking effect will increase the total energy dissipation and make the external dynamic model unconservative.

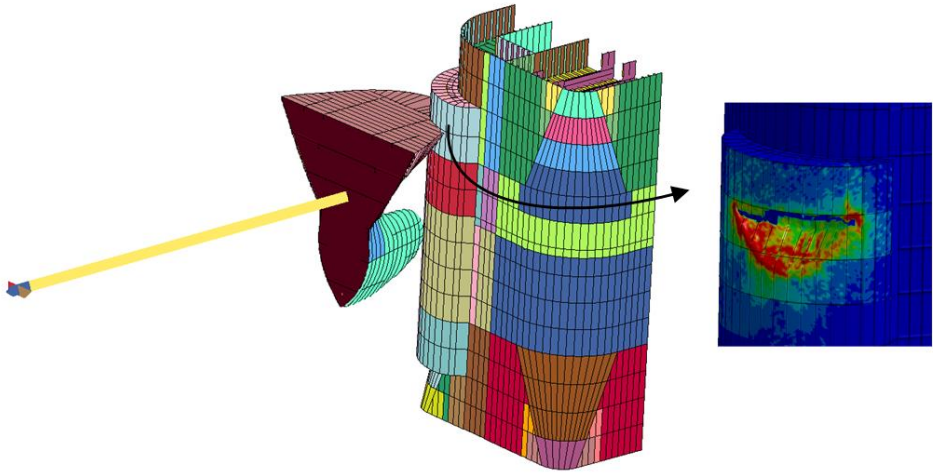

Fig. 21. Damage created in a rigid ship-deformable platform collision

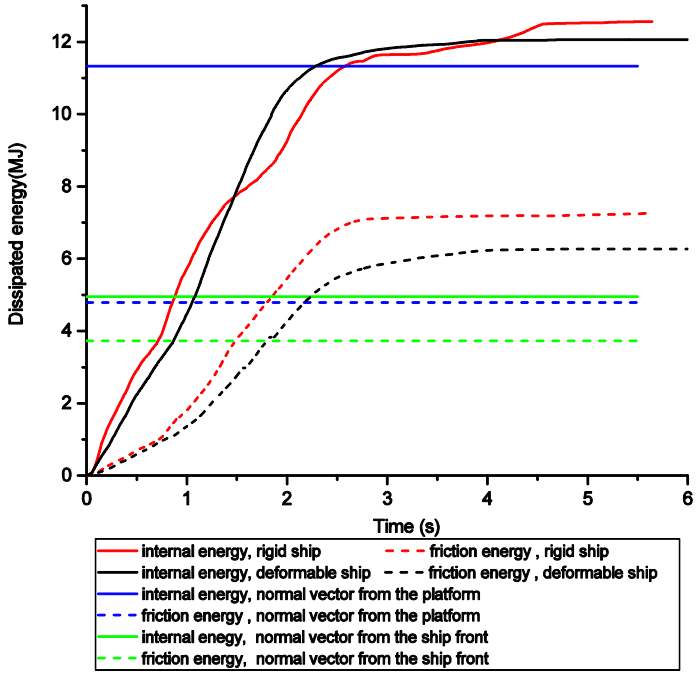

Fig. 22. Energy dissipation with coupled and decoupled methods (constant energy curves are predicted by the decoupled methods, and the others are from coupled simulations)

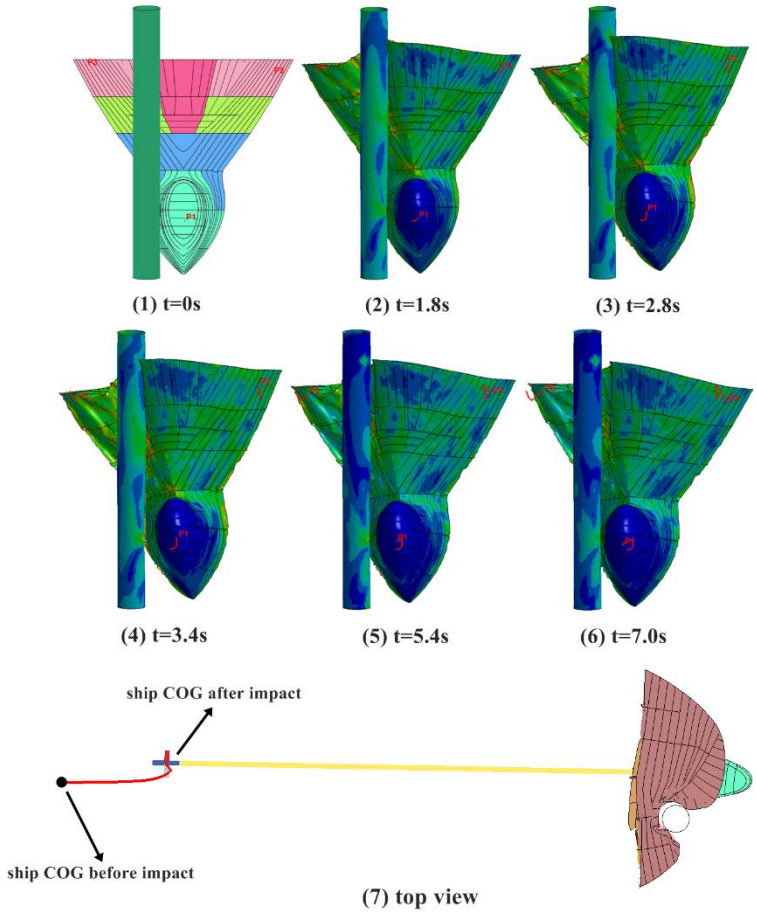

Fig. 23. Coupled simulation of a supply vessel colliding with a jacket leg

4.2.5 The assumption of the restitution factor e

The restitution factor *e* in the external dynamic models is defined as the ratio between the normal relative velocity before and after impact (see eq. (13)), which is termed as the kinematic coefficient or Newton coefficient (Newton, 1686). This enforced condition is one of the key boundary conditions for solving the motion of equations. If it is set as 0, it means that there is no relative velocity in normal direction (v_3^t=0) after the contact. It is traditionally believed to be "conservative" with respect to energy dissipation. However, zero restitution factor cannot guarantee a conservative prediction of total energy dissipation including internal and friction energy since the velocity changes on the tangential plane are not included. The variation of dissipated energy with different restitution factors using the decoupled method is shown in Fig. 24 for the 35^o collision case in scenario 1. It is observed that the internal energy reaches its maximum when *e* equals 0 and decreases with an increase of the restitution factor. However, the friction energy increases continuously with *e*. The increase is virtually linear. The total energy is maximized when a certain non-zero restitution factor is used. The value is about 0.5 in this case.

$$e = -\frac{v_3^t}{v_3^0} \tag{13}$$

In general, the restitution ratio to maximize total energy dissipation varies with cases. This ratio can be found by iterating the external dynamic program with the restitution factor ranging from 0 to 1. To be conservative without being unrealistic, it may be recommended to use a restitution factor of 0.1 for engineering practice based on observations from numerical simulations; see Table 2.

A different way to solve the problem has been proposed by Stronge (2000). He found that the use of the kinematic restitution factor in eq. (13) may lead to nonconservation of energy before and after collisions. To solve the energy inconsistence, he proposed a new definition of the coefficient termed as the energetic coefficient of restitution, see eq. (14). It is calculated from the ratio of elastic strain energy released during restitution over the internal energy during compression.

$$e_*^2 = -\frac{W_n(p_f) - W_n(p_c)}{W_n(p_c)} \tag{14}$$

where $W_n(p_c)$ is the work of normal force during compression, and $W_n(p_f)$ is the final work of normal force.

The energetic coefficient should be 0 for pure plastic impact. This definition has rarely been used in the external mechanic studies for ship or offshore structure collision problems. Further study on this aspect is recommended.

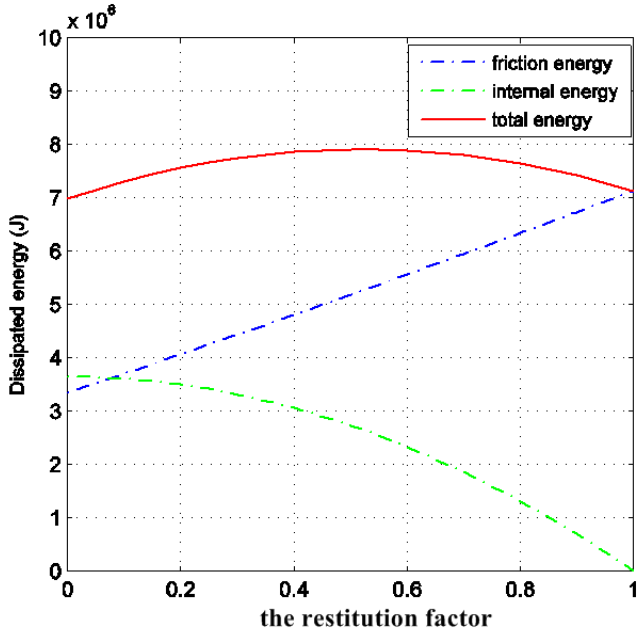

Fig. 24. Variation of dissipated energy with the restitution factor for the 35° collision case (decoupled method)

Table 2. Measured restitution factors for scenario 1 with varied collision angles

Collision angle (scenario 1)	35°	44°	56°	66°	88°
Measured restitution factor	0.19	0.18	0.12	0.08	0.08

5. Discussion of structural responses with coupled and decoupled methods

5.1 Secondary impact phenomenon

A secondary impact is observed in Fig. 17, and this is mainly due to the roll motion. During collisions, the ship normal velocity at the contact point decreases with the occurrence of sway, yaw and roll motions. The collision finishes when the relative velocity at the collision point in the normal ξ direction decreases to zero and rebound starts, i.e. $V_\xi - V_{sway,\xi} - V_{yaw,\xi} - V_{roll,\xi} \le 0$ (see Fig. 25). However, unlike sway and yaw motions, the roll motion is periodic. After $V_{roll,\xi}$ reaches its maximum, it will decrease and might change sign. This increases V_ξ again and causes a second collision to occur. The underlying mechanics also applies to cases involving the periodic heave and pitch motions.

For the 35° case of collision scenario 1, the energy carried by the roll motion is estimated to be only 0.33 MJ, which is quite small compared to dissipated total energy. However, during the period of contact loss due to roll, the yaw angle changes significantly, which changes the collision angle and yields quite different total energy dissipation; *refer Section 5.2*.

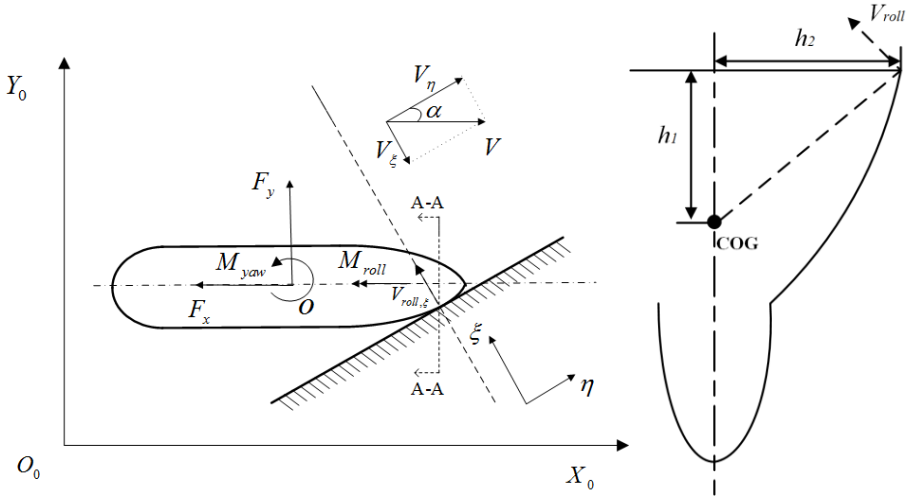

Fig. 25. Loads and velocities during collision

5.2 Energy dissipation

Fig. 26 shows the dissipated internal and friction energy curves of several typical collision cases including scenario 1 with collision angles of 35° and 56°, scenario 2 with a collision angle of 45°, and scenario 3. The initial impact velocity is 2.25 m/s. It is observed that for cases where the periodic motions are intense, e.g. scenario1-35°, secondary impacts will occur and dissipate considerable energy. The increased energy in secondary impacts mainly comes from the friction contribution while the increase of the internal energy is minor for the studied cases. The secondary impact phenomenon cannot be captured by the 3DOF coupled model. For cases where the roll velocity is small, both the 3DOF and 6DOF coupled methods predict quite similar curves as shown from the case scenario1-56° due to the counteraction effect of the lower bulbous bow.

The dissipated energy from simulations with different methods are summarized in Table 3. The dissipated total energy for scenario 1 with different collision angles is plotted in Fig. 27. It is found that for all cases, the energy dissipation predicted by the 6DOF external dynamic model agrees well with results by the 6DOF coupled model at the end of the first impact. This demonstrates the good accuracy of the decoupled method till the end of the first impact. The 3DOF external dynamic model tends to overestimate the dissipated total energy because when all the 6DOFs are released, the colliding bodies separate more easily, and more energy remains as ship kinetic energy with less energy dissipation in structural deformation. However, in cases with secondary impacts, the 6DOF external dynamic model can be unconservative since it captures only the first impact. The underestimation can be large for cases with large periodic motions; see, for example, case scenario1-35^o, scenario 2-45^o and scenario 3.

By comparing the dissipated energy at the end of the entire collision with both 3DOF and 6DOF coupled methods, it is interesting to find that although the contributions from the internal and friction energy are different, the total energy is quite close. This is because the roll motion is periodical. If the struck rigid plate is wide enough, the kinetic energy absorbed by the roll motion at the end of the first collision should be dissipated in the secondary impacts, anyhow. The internal and friction contributions are different because the collision angle changes significantly due to the large yaw motion. The conclusions agree with experimental observations in Zhang et al. (2017).

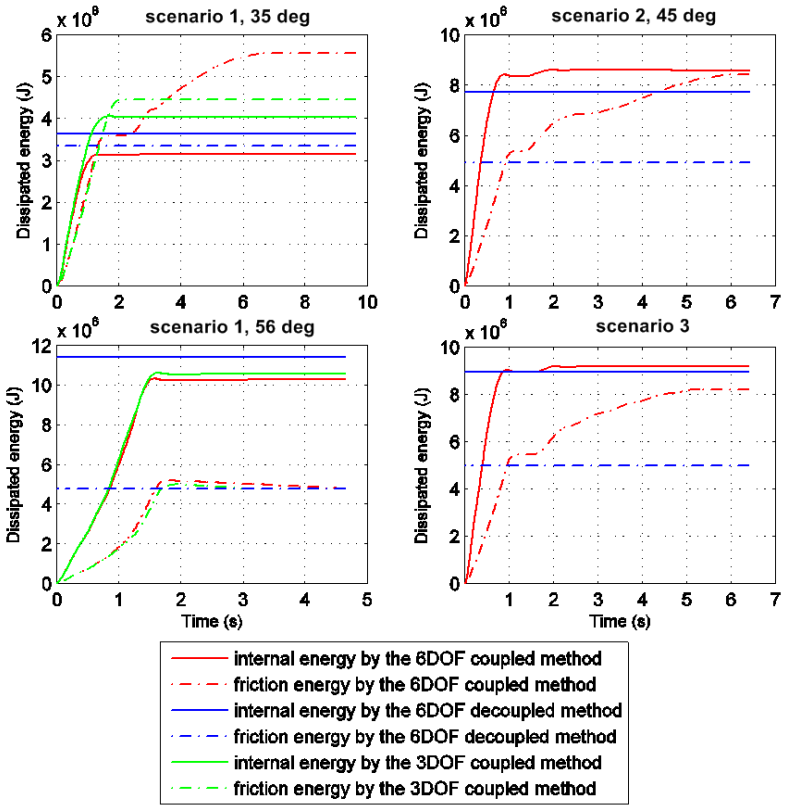

Fig. 26. Dissipated energy of several typical cases

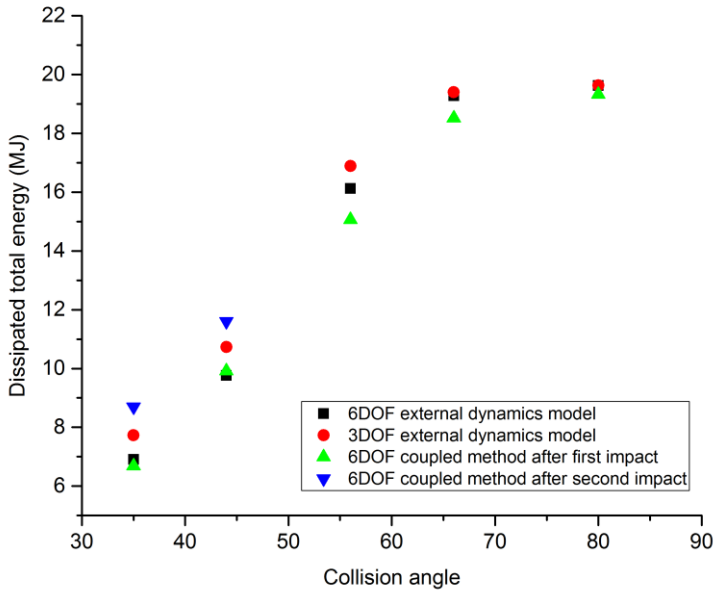

Fig. 27. The predicted total energy absorption for scenario 1 with different methods

Table 3. A comparison of dissipated energy with different methods (MJ)

Case No.	6DOF coupled method after the first impact			6DOF external dynamic model		
	internal energy	friction energy	total	internal energy	friction energy	total
Scenario1-35º	3.1	3.6	6.7	3.6	3.3	6.9
Scenario1-44º	5.4	4.6	10.0	6.3	4.3	10.6
Scenario1-56º	10.3	4.8	15.1	11.4	4.8	16.2
Scenario1-66º	14.4	4.1	18.5	16.2	3.3	19.5
Scenario1-80º	17.3	2.0	19.3	19.2	0.05	19.25
Scenario2-45º	8.3	5.4	13.7	7.7	4.9	12.6
Scenario2-60º	14.9	4.1	19.0	14.7	4.2	18.9
Scenario2-75º	18.4	1.7	20.1	19.0	0.7	19.7
Scenario3	8.9	5.5	14.4	8.9	5.0	13.9
Case No.	3DOF coupled method			6DOF coupled method after secondary impact		
	internal energy	friction energy	total	internal energy	friction energy	total
Scenario1-35º	4.0	4.4	8.4	3.2	5.6	8.8
Scenario1-44º	6.6	5.1	11.7	5.4	6.2	11.6
Scenario1-56º	10.6	4.8	15.4	--	--	--
Scenario1-66º	14.6	4.1	18.7	--	--	--
Scenario1-80º	17.4	2.1	19.5	--	--	--
Scenario2-45º	--	--	--	8.6	8.4	17.0
Scenario2-60º	--	--	--	--	--	--
Scenario2-75º	--	--	--	--	--	--
Scenario3	--	--	--	9.2	8.2	17.4

-- Not applicable

5.3 Ship motions and structural damage

Fig. 28 presents ship motions for collision scenario 1 evaluated by the decoupled method in which the struck object is kept stationary while the striking object has prescribed displacement, the 3DOF coupled method and the 6DOF coupled method. The markers on the curves represent time instants when the collision finishes. For the decoupled method, a collision ends when the energy calculated from external dynamics models is dissipated through structural deformations in the assessment of internal mechanics. For the coupled method, a collision completes when collision forces decrease to zero. Curves with two markers represent cases with secondary impacts.

It is observed that the decoupled approach predicts deeper penetrations normal to the contact plane but shorter transverse extent. The deviation is especially obvious for cases with small collision angles. The extent of transverse damage is underestimated by about 50% for the 35°, 44°, 56° and 66° impact cases, where the striking ship and the rigid plate slide over each other. The deviation is small for cases with large collision angles, e.g. scenario1-80°. In cases with secondary impacts, the decoupled method is not able to capture a second collision. As ship structures are not homogeneous in general, the responses of structures can be different given a different collision path. Tabri and Broekhuijsen (2011) compared deformation energy required to breach an inner hull using the decoupled method and a coupled method. They found that the difference in deformation energy with the two methods could be up to 90% due to the path deviation.

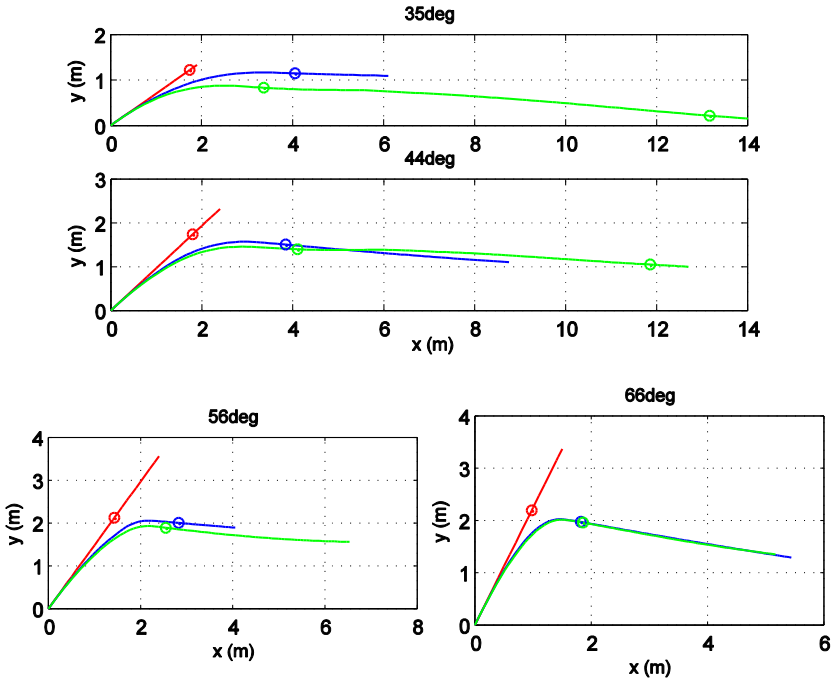

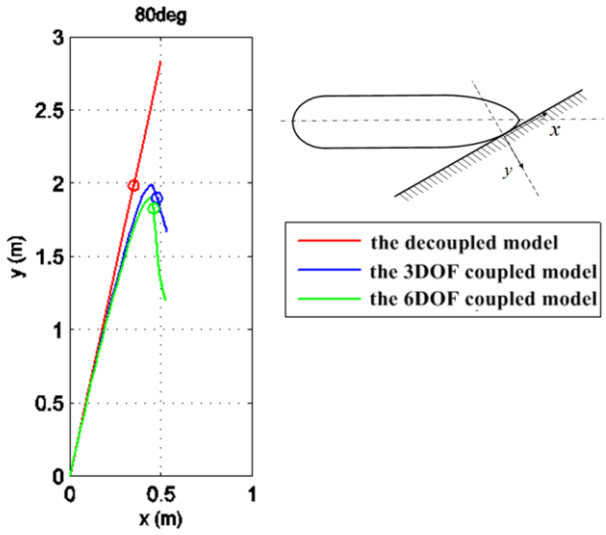

Fig. 28. Global motions of the striking ship

The path deviation is mainly induced by the yaw motion with little contribution from the roll motion, but the periodical motions can induce secondary impacts and should not be neglected. Fig. 29 shows the damage extent when the supply vessel collides with a cylindrical column of a semi-submersible platform. The penetration normal to the collision plane is shallower with the coupled method, and the tangential damage extension is larger. The deformation is elliptical with the coupled method rather than circular with the decoupled method. The coupled approach predicts more realistic penetration paths and structural damage. In view of possible large prediction deviations of energy dissipation and structural damage using the decoupled method, it is suggested to verify the critical cases with the coupled method.

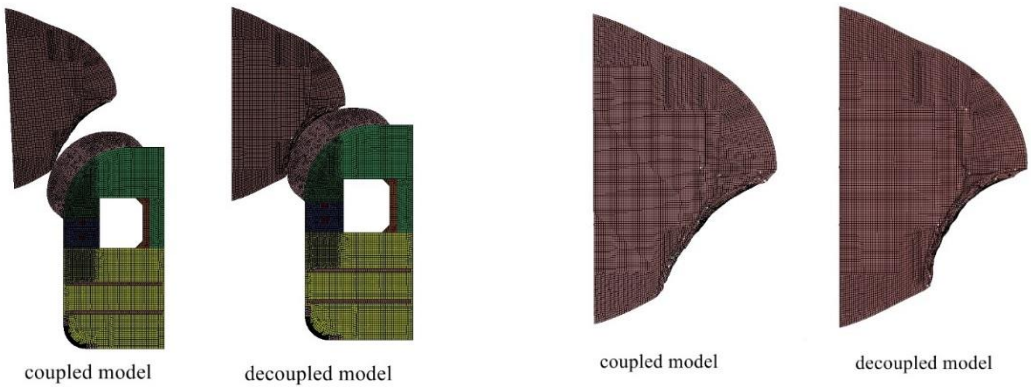

Fig. 29. Structural damage with the coupled and decoupled method at the end of the collision

5.4 Influence of the forward speed effect

The influence of forward speed effect is studied with the coupled model 2 up to a high collision velocity. The 'forward speed effect' here is defined from a hydrodynamic point of view. Second-order terms are induced by the ship forward speed as explained in *Section 2.2* in contrast to the first-order seakeeping theory. This section is to check if the second order terms of hydrodynamic loads induced by the forward speed have big influence on the ship motions during collisions.

Fig. 30 shows a comparison of ship motions with and without considering the second order forward speed effect for the collision scenario 4. The speed is 5.56 m/s corresponding to a Froude number of 0.2 and a kinetic energy of 116 MJ. Here t=0 represents the instant when the colliding bodies start to crush each other.

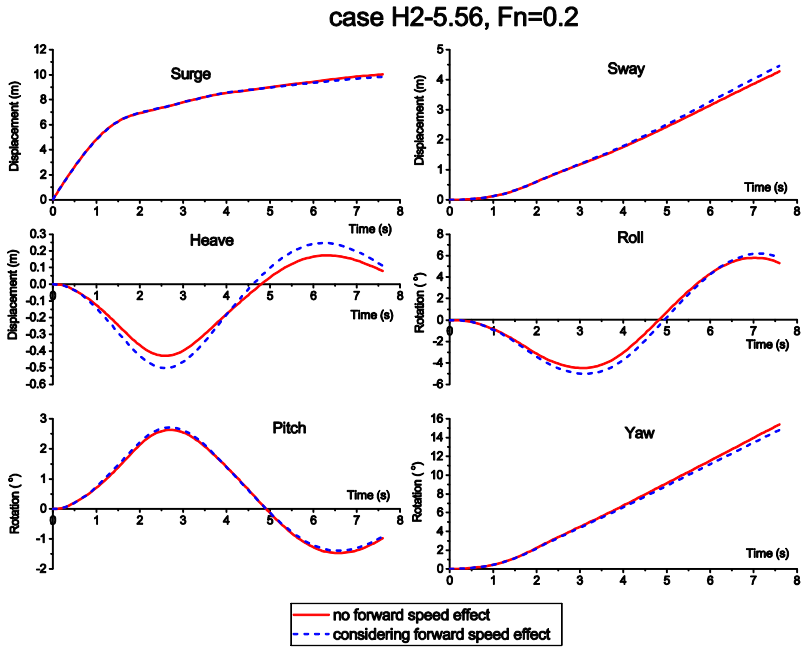

Fig. 30. Ship motions with a collision velocity of 5.56 m/s

The influence of the second order forward speed effect is found to be limited up to a Froude number of 0.2, which is a significant speed for most collision scenarios. Consequently, it is concluded that the first order potential-flow theory for seakeeping problems is sufficiently accurate for most collision and grounding scenarios if no incident waves are assumed.

6. Conclusions

This paper reviews assumptions and simplifications of external dynamic models, and verifies the assumptions by comparing with 3DOF and 6DOF coupled simulation results. The influence of coupling between fluid and structures, and between ship motions and structural deformations is discussed. The following conclusions are drawn:

1. The equivalent added masses vary with the shape of the collision curve, the collision duration, and the definition. The frequency content of collision forces is quite dispersive, and it is difficult

to find a representative frequency to determine the constant added mass for the external dynamics models. However, the varying added mass coefficients in sway and yaw were found to have little influence on the total energy absorption for large collision angle cases. In these cases, values that are typically used in present design guidance may be appropriate. The influence tends to become more important with decreasing collision angles.

2. The collision angle is assumed to be constant during collisions in external dynamics models. For short duration collisions, this is reasonable; but for cases with long durations or secondary impacts, the collision angle may change significantly, leading to large discrepancies with respect to energy dissipation and ship trajectories.

3. The impact mechanics models assume collisions between rigid bodies, which share a common tangential plane. However, in practice, the structures are deformable and often do not have a common tangential plane before impact. This makes it difficult to determine the normal vector of the contact plane as input of the external dynamics model. It requires good engineering judgements to determine the appropriate normal vector. Failure to identify the correct normal vector will yield erroneous results. From the limited simulation results, it may be recommended to use the normal vector of the initial surface of the stronger structure as input for open structures, where 6DOF motions are not restricted by structural deformations. For nonopen and nonconvex structures, ship motions may be locked by structural deformations, and the 3DOF external dynamic model neglecting the roll motion is recommended for conservative consideration. More investigation is needed on this aspect.

4. It is not necessarily conservative to assume a restitution factor of 0 if the traditional kinematic restitution factor is used. It is recommended to use 0.1 for engineering use if the rebound velocity is unknown. Further, the traditional definition of restitution has energy inconsistence problem and should be used with caution. Alternatively, the energetic restitution factor can solve the energy inconsistence problem and should be further investigated.

5. The periodic motions of roll, pitch and heave may induce secondary impacts in ship collisions and groundings, which may increase the total energy dissipation significantly.

6. The 6DOF decoupled method is found to be capable of predicting the energy dissipation till the end of the first impact period with reasonable accuracy. However, up to this point, structural damage cannot be predicted with the same accuracy. Deviation of predicted damage in the transverse direction can be large, especially for cases with small collision angles. Secondary impacts are not captured by the decoupled models.

Acknowledgments

This work has been funded by the Research Council of Norway (NFR) through the Centers of Excellence funding scheme, project AMOS (Grant number 223254) at the Norwegian University of Science and Technology (NTNU). This support is gratefully acknowledged by the authors.

References

BROWN, A. J. 2002. Collision scenarios and probabilistic collision damage. *Marine Structures,* 15**,** 335-364.

FERRY, M. 2001. MCOL User's Manual. *Principia Marine, Nantes*.

HONG, L. 2009. Simplified analysis and design of ships subjected to collision and grounding. *PhD Thesis, Norwegian University of Science and Technology, Norway*.

JIA, H. & MOAN, T. Global Responses of Struck Ships in Collision With Emphasis on Hydrodynamic Effects. ASME 2010 29th International Conference on Ocean, Offshore and Arctic Engineering, 2010. American Society of Mechanical Engineers, 225-236.

LE SOURNE, H., BESNARD, N., CHEYLAN, C. & BUANNIC, N. 2012. A Ship Collision Analysis Program Based on Upper Bound Solutions and Coupled with a Large Rotational Ship Movement Analysis Tool. *Journal of Applied Mathematics,* 2012**,** 27.

LE SOURNE, H., DONNER, R., BESNIER, F. & FERRY, M. External dynamics of ship-submarine collision. Preprints of 2nd International Conference on Collision and Grounding of Ships, Copenhagen, 2001.

LIU, Z. & AMDAHL, J. 2010. A new formulation of the impact mechanics of ship collisions and its application to a ship–iceberg collision. *Marine Structures,* 23**,** 360-384.

MARINTEK 2012. SIMO - User's manual Version 4.0 rev0. *Marintek Report*.

MINORSKY, V. 1958. An analysis of ship collisions with reference to protection of nuclear power plants. Sharp (George G.) Inc., New York.

MOTORA, S., FUJINO, M., SUGIURA, M. & SUGITA, M. 1971. Equivalent Added Mass of Ships in Collisions. *Selected papers from the journal of the Society of Naval Architects of Japan,* 7**,** 138-148.

NEWTON, I. 1686. Principia: Mathematical Principles of Natural Philosophy (and His System of the World)(1686). Reprinted by Univ. of CA Press.

NORRBIN, N. H. 1971. Theory and observations on the use of a mathematical model for ship manoeuvring in deep and confined waters. DTIC Document.

OSHIRO, R. E., CALLE, M. A. G., MAZZARIOL, L. M. & ALVES, M. 2017. Experimental study of collision in scaled naval structures. *International Journal of Impact Engineering*.

PEDERSEN, P. T. & ZHANG, S. 1998. On impact mechanics in ship collisions. *Marine Structures,* 11**,** 429-449.

PETERSEN, M. J. 1982. Dynamics of ship collisions. *Ocean Engineering,* 9**,** 295-329.

PETERSEN, M. J. & PEDERSEN, P. T. Collisions between ships and offshore platforms. Offshore Technology Conference, 1981. Offshore Technology Conference.

PILL, I. & TABRI, K. 2011. Finite element simulations of ship collisions: A coupled approach to external dynamics and inner mechanics. *Ships and Offshore Structures,* 6**,** 59-66.

POPOV, Y. N., FADDEEV, O., KHEISIN, D. & YAKOVLEV, A. 1969. Strength of ships sailing in ice. DTIC Document.

SAMUELIDES, E. & FRIEZE, P. 1989. Fluid-structure interaction in ship collisions. *marine Structures,* 2**,** 65-88.

STRONGE, W. J. 2004. *Impact mechanics*, Cambridge university press.

TABRI, K. 2012. Influence of coupling in the prediction of ship collision damage. *Ships and Offshore Structures,* 7**,** 47-54.

TABRI, K. & BROEKHUIJSEN, J. Influence of ship motions in the numerical prediction of ship collision damage. Advances in Marine Structures - Proceedings of the 3rd International Conference on Marine Structures, MARSTRUCT 2011, 2011. 391-397.

TABRI, K., BROEKHUIJSEN, J., MATUSIAK, J. & VARSTA, P. 2009. Analytical modelling of ship collision based on full-scale experiments. *Marine Structures,* 22**,** 42-61.

TABRI, K., VARSTA, P. & MATUSIAK, J. 2010. Numerical and experimental motion simulations of nonsymmetric ship collisions. *Journal of Marine Science and Technology,* 15**,** 87-101.

TRAVANCA, J. & HAO, H. 2014. Dynamics of steel offshore platforms under ship impact. *Applied Ocean Research,* 47**,** 352-372.

VAN BERLEKOM, W. B. & GODDARD, T. A. 1972. Maneuvering of large tankers. *Presented at the Annual Meeting of SNAME, Society of Naval Architects and Marine Engineers,* Paper #8.

WANG, L., YANG, L., HUANG, D., ZHANG, Z. & CHEN, G. 2008. An impact dynamics analysis on a new crashworthy device against ship–bridge collision. *International Journal of Impact Engineering,* 35**,** 895-904.

YU, Z. & AMDAHL, J. 2016. Full six degrees of freedom coupled dynamic simulation of ship collision and grounding accidents. *Marine Structures,* 47**,** 1-22.

YU, Z. & AMDAHL, J. 2018. A review of structural responses and design of offshore tubular structures subjected to ship impacts. *Ocean Engineering,* 154**,** 177-203.

YU, Z., AMDAHL, J. & STORHEIM, M. 2016a. A new approach for coupling external dynamics and internal mechanics in ship collisions. *Marine Structures,* 45**,** 110-132.

YU, Z., SHEN, Y., AMDAHL, J. & GRECO, M. 2016b. Implementation of Linear Potential-Flow Theory in the 6DOF Coupled Simulation of Ship Collision and Grounding Accidents. *Journal of Ship Research,* 60**,** 119-144.

ZHANG, S., VILLAVICENCIO, R., ZHU, L. & PEDERSEN, P. T. 2017. Impact mechanics of ship collisions and validations with experimental results. *Marine Structures,* 52**,** 69-81.

Appendix. Practical guidance on the use of the user subroutines for the implementation of the 6DOF coupled models

The user defined load subroutine (LOADUD) and the user common subroutine (USERCOMM) in LS-DYNA have been used in limited applications. The running company of the software, LSTC, does not provide much information on how these subroutines should be used, and very few relevant references can be found from the literature. Users of the subroutines have to familiarize themselves through trial and error. The present appendix summarizes the experience of using the subroutines by the first author during the implementation of hydrodynamic forces. This will hopefully provide useful guidance for those who also wish to use the subroutines to implement the hydrodynamic forces or other user defined forces. Note that the encountered problems and solutions presented below are based on the first author's own experience, and do not reflect the official view of LSTC.

1. To implement the linear potential flow theory, velocity history and external impulse response functions should be stored, while LOADUD provides information only in the current timestep. As a solution, the USRCOMM subroutine provides variables which can store the velocity history and external information as matrices. The information will not be erased upon moving to next timestep.

2. Nodal accelerations in LOADUD are only available for deformable bodies, but not for rigid bodies. This may be due to special treatment of rigid bodies in LS-DYNA. If a deformable body is used to represent the hull girder, the girder will generate large structural vibrations and significant oscillations of nodal accelerations, leading to divergence. To solve this acceleration problem, the USERCOMM subroutine is used to track the velocity history of nodes on rigid beams. The nodal accelerations in Yu et al. (2016a), Yu and Amdahl (2016) and Yu et al. (2016b) are then approximated as:

$$a_n = \frac{V_n - V_{n-2}}{t_n - t_{n-2}} \tag{A.1}$$

   More coupled simulations showed that it was not always credible to use Eq. (A.1). For some cases, the code converges successfully while in some cases the estimated accelerations and corresponding added mass forces will have a backward coupling with the main solver and yield velocity oscillations and numerical instabilities. An improvement to this is to fit a linear velocity curve to the raw data as plotted in Fig. A-1. The backward coupling with the main solver is prevented when the accelerations are not estimated by going through the exact velocity points, but are satisfied in an average level.

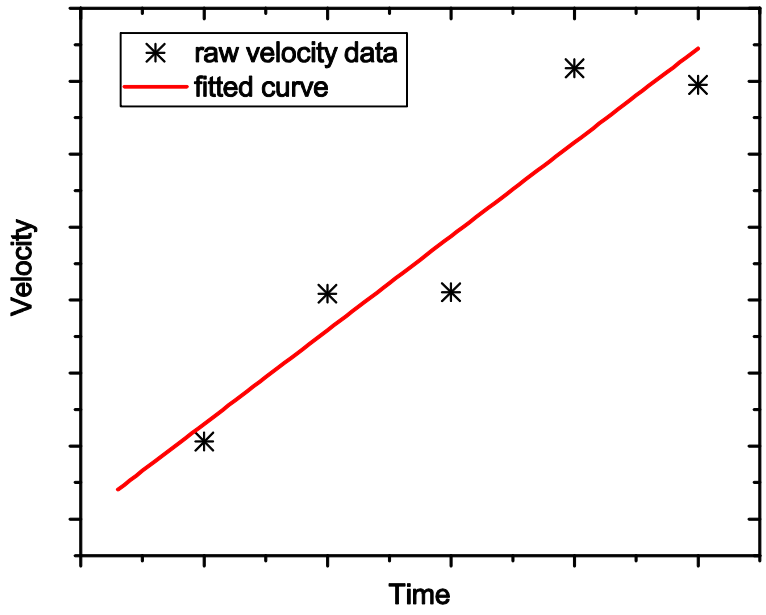

Fig. A-1. The fitted velocity curves

3. The LOADUD subroutine gives the following description for a beam element:

```
c     ixb - beam  element connectivities (ixb(1,*)=part ID)
c                                        (ixb(2,*)=node 1)
c                                        (ixb(3,*)=node 2)
c                                        (ixb(4,*)=orientation node)
```

   Based on the information, one can hardly locate the correct node, on which one wishes to apply the user loads. It is found that the numbering system of nodes, beam elements and shell elements in the subroutines are different from that in the finite element model. This makes it very difficult to find the correct representation of the target element in the user subroutine.

   To find the correct node and beam element for applying the user forces, we used the 'write' sentence to output the information of all beam elements, compared with the information in the FE model and finally found the correct number for the target beam elements and nodes.

4. LOADUD does not provide options to apply bending moments directly on a rigid beam, so the bending moments should be transformed into force pairs. Therefore, several small beams are created for applying bending moments in roll, pitch and yaw as shown in Fig. 4. The angular velocity and acceleration are also not provided, and they should be obtained from nodal velocities.

5. Constant time step should be maintained during the calculations for two reasons:

   (a). The velocity history is stored to approximate nodal accelerations and to make convolution integrals. A time-varying timestep can make the problem much more complicated, where the

corresponding timestep history must be tracked and stored, and the approximated acceleration may not be stable.

(b). The impulse response functions should be written in a text file with a certain time interval. It is difficult to prepare the file with a time varying time interval, which is not predictable before the calculation.

The constant time step can be enforced using the mass-scaling technique. Mass-scaling refers to a technique whereby nonphysical mass is added to a structure in order to achieve a larger explicit timestep. Added masses less than 5 percent of total mass may be considered to have little influence on the accuracy of simulation results.

6. The timestep is normally in the order of 10^{-6} s for explicit ship collision simulations, which is too small to change the hydrodynamic forces during the period. It is therefore unnecessary to update the hydrodynamic forces in each structural iteration timestep. In the present simulation, the hydrodynamic forces are updated every 400 timesteps of structural analysis iterations, corresponding to a time interval of 0.001s. This makes the method very efficient but still preserves good accuracy.
7. LS-DYNA does not allow direct connection of rigid bodies. They should be defined as master and slave parts through the card *CONSTRAINED_RIGID_BODIES.
8. The error of ‘stack overflow’ is often encountered with the user compiled executable solver. This can be solved by increasing the stack size in the ‘makefile’ of the library package.